

Software defined radio implementation of passive RADAR using low-cost DVB-T receivers

W. Feng*, G. Cherniak*, J.-M. Friedt[†]*, M. Sato *

*Center for NorthEast Asian Studies (CNEAS), Tohoku University, Sendai, Japan

[†]FEMTO-ST, Time & Frequency department, Besançon, France

Email: jmfriedt@femto-st.fr, motoyuki.sato.b3@tohoku.ac.jp

Abstract—Software Defined Radio (SDR) is redefining how a broader public has access to radiofrequency devices by moving processing steps from hardware to software. The flexibility of SDR receivers allows for the use of a single affordable hardware in a wide range of fields, including communication, time transfer or electromagnetic wave propagation conditions. By synchronizing multiple receivers, non-cooperative radiofrequency sources are used for passive radar applications in which the radiofrequency wave reflected by targets is analyzed to recover range and velocity informations. We investigate the use of low-cost Digital Video Broadcast-Terrestrial (DVB-T) receivers used as general purpose SDR for passive radar applications. We demonstrate the detection of static and moving targets as well as short range targets. Technical challenges of diverting consumer electronics for passive radar applications are discussed.

I. DIGITAL VIDEO BROADCAST-TERRESTRIAL RECEIVERS AS GENERAL PURPOSE SOFTWARE DEFINED RADIO RECEIVERS

Moving hardware functions to software has been an ongoing trend driven on the one hand by the flexibility and reconfigurability of software with respect to hardware, but also in the consumer electronics by the ability to lower cost. Communication modems – so called winmodems or softmodems – have followed this trend in the 1990s, and now radiofrequency reception peripherals are as well. Porting the driver of a Digital Video Broadcast-Terrestrial (DVB-T) receiver to the Linux operating system led, in 2010 [1], to the discovery that Realtek RTL2832U based DVB-T receivers were actually general purpose Software Defined Radio (SDR) receivers. Their broad availability and low cost made them popular with amateur SDR enthusiasts, including those using the opensource GNURadio (www.gnuradio.org) SDR-framework: the DVB-T receivers are supported as I, Q coefficient sources with bandwidths up to 2.4 Msamples/s and 8-bit resolution, well suited for many analog and low-bandwidth digital communication modes, and making them ideally adapted for educational material. Since 2010, several radiofrequency frontends in charge of radiofrequency signal amplification and transposition to baseband (direct conversion) have been available, initiated with the now defunct Elonics E4000 and with the latests versions using the Rafael Micro R820T2, at a unit cost of about 10 euros or 1200 yens. We consider using such low-cost SDR receivers to illustrate radar processing techniques to a wide audience.

Active radar measurements are limited to a few professional organisations by the legal and technical requirements associated with high power, broadband emitters. Indeed, radar signals decay as the squared distance between source and target multiplied by the squared distance between target and receiver, similar to the fourth power decay with distance of monostatic radar power, requiring stronger emission powers than one-way

radiofrequency communication applications. A radar range resolution is inversely proportional to its bandwidth, so that broadband signals are needed for high range resolution. An alternative to using a dedicated radar emitter is to use the many radiofrequency signal sources already deployed for various purposes: analog television, commercial broadcast FM, mobile phone or digital communication networks such as Wifi. One of the sources meeting the high power and wide bandwidth requirement for radar applications is digital television: in Sendai (Japan), three television towers emit signals with a power of 3 kW on frequencies ranging from 470 to 570 MHz (Fig. 1). We use the 509 MHz channel allocated to the Tohoku Broadcasting Company. Using non-cooperative sources for mapping targets is the field of multistatic passive radars.

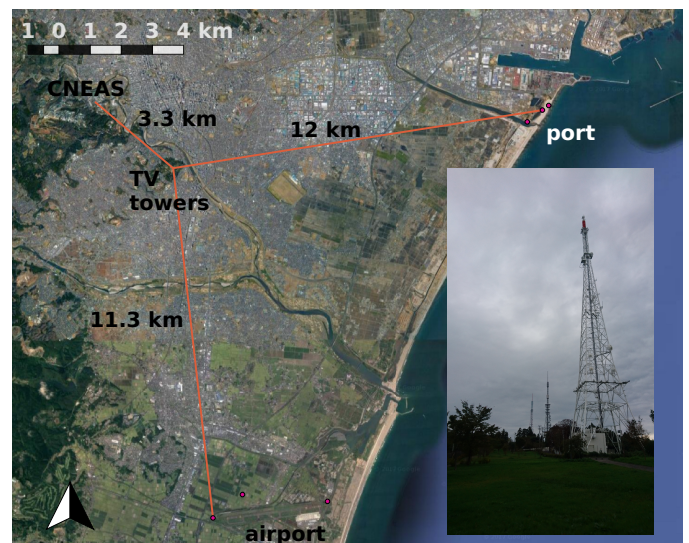


Fig. 1. Three TV towers located at 3.3 km from the CNEAS laboratory, 12 km from the port and 11.3 km from the airport, broadcast radiofrequency signals over Sendai used for passive radar experiments. Background map: Google Maps.

The underlying requirement for passive radar application is to measure on the one hand the signal emitted by the non-cooperative source, called the reference signal, and on the other hand the signal reflected by targets. Since the reference signal is not known, a matched filter approach is required to find delayed copies of this reference signal in the measured signal: a cross-correlation technique allows for identifying the time delayed copies of the reference in the measurement. Since the non-cooperative source is not a noise generator exhibiting a flat spectrum but transmits some structured information which might repeat in time or frequency, analyzing the spectral characteristics of the source is needed to assess its suitability for passive radar application: this analysis yields the ambiguity function [2]. Since a target moving at velocity v introduces a

Doppler shift f_D on the reflected signal $f_D = 2f_0 \frac{v}{c}$ with f_0 the carrier frequency and c the velocity of electromagnetic waves, cross correlating the reference signal ref time-shifted by τ with respect to the measurement signal $meas$ frequency-shifted by f_D naturally yields the ambiguity function

$$|amb(\tau, f_D)|^2 = \left| \int_{-\infty}^{+\infty} ref(t + \tau) \cdot meas^*(t) \exp(j2\pi f_D t) dt \right|^2 \quad (1)$$

with $j^2 = -1$ and the $*$ symbol indicating the complex conjugate. Ideally the ambiguity function would be a Dirac function if target detection in the range-Doppler plan was unambiguous: practical sources will exhibit some redundancy in the time or frequency domain that might be erroneously interpreted as detected targets. The ambiguity function of the source, by autocorrelating the reference signal with its Doppler-frequency shifted copies, provides the information on the redundancy needed to prevent false target detection (Fig. 2). The ambiguity function of various sources have been documented in [3], [4].

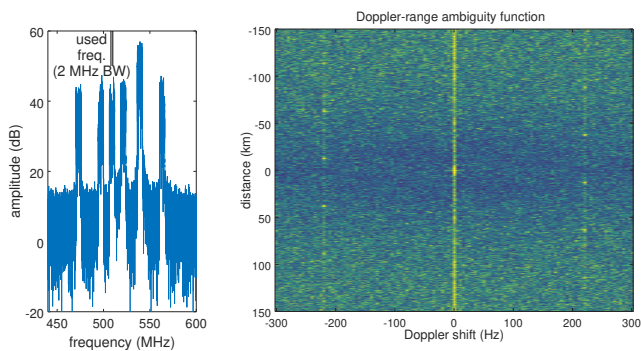


Fig. 2. Left: spectrum of the six terrestrial digital television stations broadcasting in Sendai. Right: ambiguity function of the signal emitted for broadcasting digital television signals in Japan (ISDB-T). The information at ± 210 Hz offset from the carrier should not be mistaken for targets.

II. REQUIREMENTS OF COHERENT MEASUREMENTS

Multiple authors have demonstrated the ability to perform coherent measurements with two DVB-T receivers clocked by a common clock [5], [6], [7], [8] but we have not found a formal and detailed description of the procedure followed to acquire their data. Finding time-delayed copies of the reference signal in the measurement signal requires three conditions: the local oscillator of both radiofrequency receivers must be coherent over the duration of the analysis, the data transferred by the two receivers must be synchronous, and the direct wave reaching the measurement receiver must not overwhelm the weak reflections from distant targets. Using two consumer electronic DVB-T receivers with the local oscillator of one of the receivers used as a clock for the second receiver might seem to provide the solution (Fig. 3).

However, in the case of consumer electronics DVB-T receivers, the quartz oscillator is set at the USB-bus clock frequency and multiplied by a phase locked loop (PLL) by the radiofrequency front-end to reach the targeted carrier frequency. This PLL suffers two issues for coherent measurements: dithering allows fine frequency steps but introduces some phase coherence loss, and temperature dependence of the PLL behaviour introduces some phase drift of one receiver with respect to the other. The frequency dithering, active as a default configuration of the `librtlsdr` library found in the Debian distribution of Linux (Fig. 4), is deactivated by

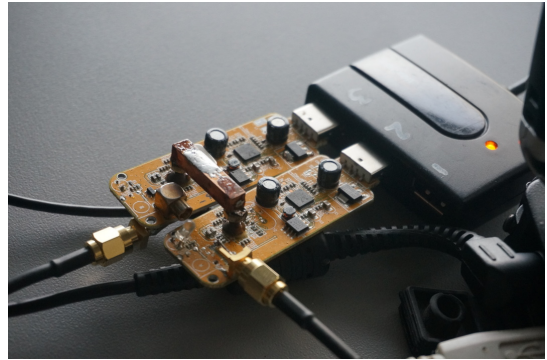


Fig. 3. Experimental setup, with a thermal link made of a copper beam between the two radiofrequency frontends. The reference oscillator output from one receiver feeds the clock signal of the other receiver.

modifying the software according to [9] and compiling a custom version of the `osmosdr` GNURadio source block linked against this updated library.

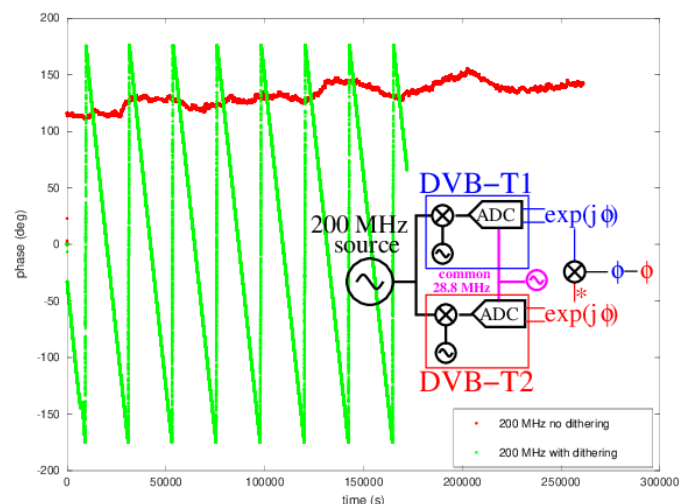


Fig. 4. Impact of dithering (green active, red deactivated) on the phase difference between the output of two DVB-T receivers fed by the same oscillator.

Temperature drift is tackled by providing some thermal link between the two receiver frontends (Fig. 3). The data transmission synchronization is addressed at the post-processing level. DVB-T receivers communicate over a USB-bus: the latency between two measurement initialization sequences cannot be predicted. Indeed, the datastream start time has been observed to randomly vary as GNURadio triggers the measurements from both dongles asynchronously. However, once the datastream was started, and for datarates below 2.048 Msamples/s, the time offset was observed to be constant and no sample loss was observed. The time offset between the two streams is observed to be most of the time in the $\pm 500 \mu s$ range (Fig. 5), or ± 1000 samples when sampling at 2 MS/s.

Since a fraction of the reference signal always leaks on the measurement channel, identifying the time delay is possible. However, this initial calibration only remains valid as long as the datastream remains uninterrupted.

III. DEMONSTRATION WITH STATIC TARGET DETECTION

Considering the basic setup and processing sequence has been described, we now demonstrate a measurement using the setup described above, with a fixed 18 element Yagi-Uda pointing towards the reference signal and the azimuth

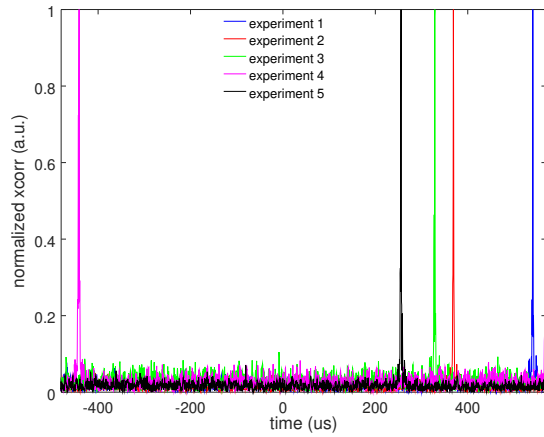


Fig. 5. Normalized cross-correlation between the reference and measurement receivers both connected to the same antenna: the time delay between the two streams randomly varies from one measurement to another, but remains most of the time in the $\pm 500 \mu\text{s}$ range.

of the 18 element measurement Yagi-Uda antenna scanning a 170° range. Since static targets are considered, the Doppler frequency shift is set to 0 and the ambiguity function Eq. 1 becomes a cross-correlation calculation. An example is given in Fig. 6: GNURadio allows for real time display of the cross-correlation as data are acquired, a key feature with respect to post-processing to make sure the collected data are usable while in the field.

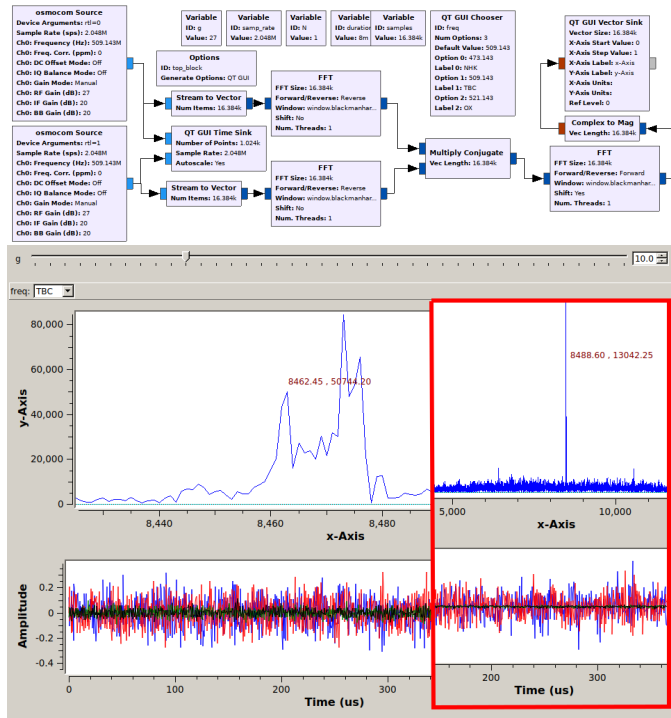


Fig. 6. Top: simplified flow GNURadio flowchart for real-time processing the cross-correlation between two DVB-T receiver sources. Bottom the resulting charts during execution, with at the bottom the real (blue, red) and imaginary (dark colors) parts of the reference and measurement signals. Top is the zoom on the cross correlation peak, showing fine features beyond the large-cross correlation peak exhibited on a wider range in the inset.

The real time correlation is displayed by converting the continuous stream to vectors, computing the Fourier transform of each vector, then computing the product of one resulting vector with the complex conjugate of the other vector,

and finally taking the inverse Fourier transform, based on the consideration that the Fourier transform of the cross-correlation x is the product of the Fourier transform FT of the reference channel multiplied by the complex conjugate of the measurement channel

$$x(ref, meas)(\tau) = FT^{-1}(FT(ref) \cdot FT^*(meas))$$

All these processing steps are available as processing blocks in GNURadio and are readily implemented for real time analysis (Fig. 6).

Fig. 7 illustrates the resulting map, with a returned signal maximum in the azimuth of the nearest buildings. However, the poor range resolution associated with the low measurement bandwidth only provides a coarse spatial resolution for such short range measurements.

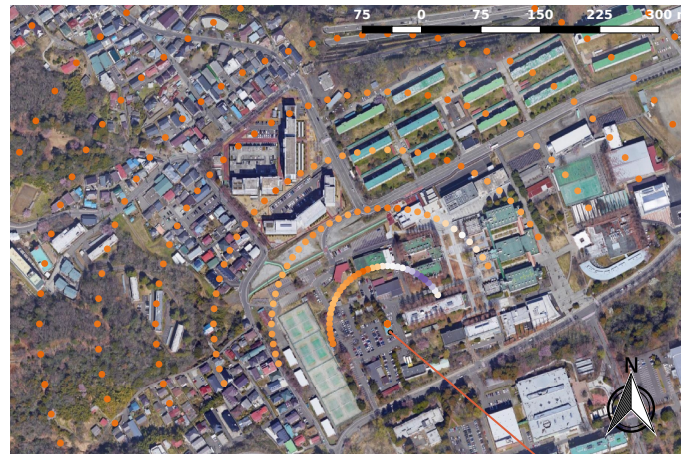


Fig. 7. Cross-correlation magnitude as a function of azimuth and range. The low DVB-T receiver bandwidth only yields a sparse mapping of possible reflectors as surrounding buildings.

Replacing the DVB-T receiver with a radiofrequency-grade oscilloscope, using an external amplifier and down-converter, yields consistent but much sharper map of the power reflected by the surrounding buildings (Fig. 8). The flexibility of GNURadio and SDR is demonstrated with the ease with which the low-bandwidth DVB-T source is replaced by a digital oscilloscope, as demonstrated with the <https://github.com/jmfriedt/gr-oscilloscope> example: the lack of continuity of the signal recorded from the oscilloscope does not prevent radar applications but prevents continuous streams to be analyzed.

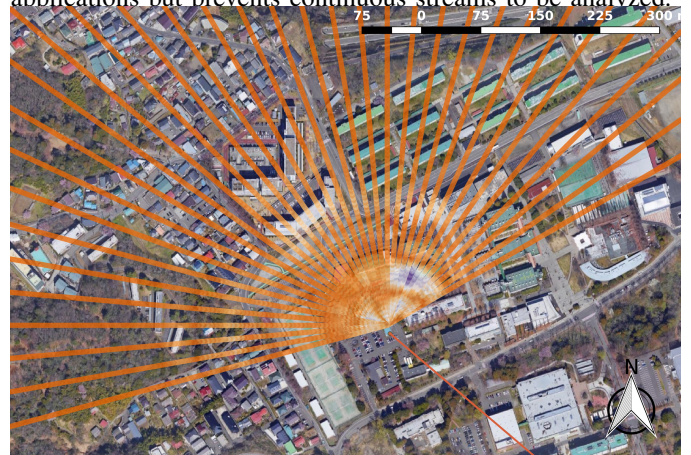


Fig. 8. Cross-correlation magnitude as a function of azimuth and range using a radiofrequency- grade oscilloscope as receiver. The map of reflectors becomes sharper, and consistent with Fig. 7.

IV. APPLICATION TO MOVING TARGET DETECTION

Far range measurement of moving targets benefits from the Doppler frequency shift introduced by the target motion to differentiate it from static clutter – part of the classic Moving Target Identification (MTI) filter. We demonstrate moving target detection on the range-Doppler plane on two aircrafts and ships, the former exhibiting large velocities even at the landing stage of the flight, and the latter smaller velocities but larger radar cross section (RCS).

A. Airplane detection

The acquisition parameters are defined by the characteristics of the target: considering we observe planes in the final stage of landing, we assume a flight velocity of at most 360 km/h, introducing a Doppler frequency shift of 333 Hz on the 500 MHz carrier. On the other hand the 2 MHz wide analysis bandwidth only allows for 75 m range resolution: a plane flying at 360 km/h covers 75 m in 750 ms. We hence select a tradeoff between Doppler frequency resolution, range resolution and computational power by selecting 125 ms-long data segments, providing a 8 Hz Doppler frequency resolution during which the plane travels 12 m at most. The plane becomes visible far from clutter at a bistatic range of about 8 km (Fig. 9).

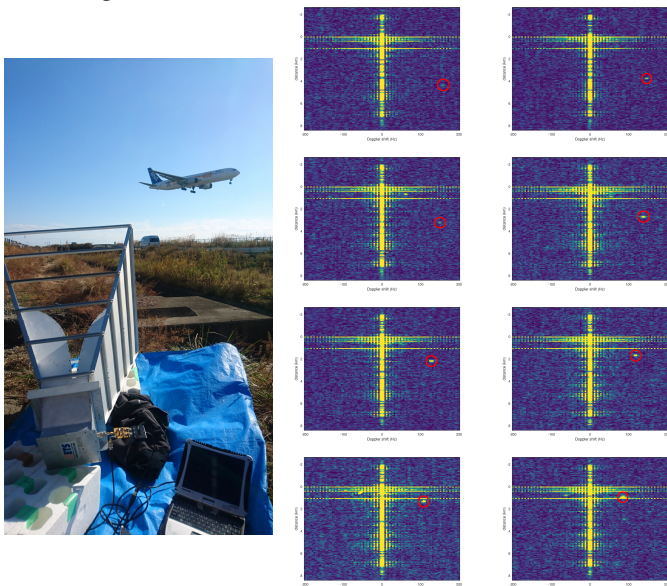


Fig. 9. Left: picture of a plane landing in front of the antenna collecting the measurements. Right: evolution of the range (Y-axis)-velocity (X-axis) map over time as the plane approaches and lands. The red dot indicates the moving target, the bright cross being the clutter sidelobes in the range and velocity directions. Time evolves from top-left (plane furthest from landing strip at the lower-right of the picture) to bottom-right (plane over the landing strip).

Increasing the integration time to the optimum 0.5 s segments increases computation time but lowers sidelobes and improves signal to noise ratio by improved pulse compression: low RCS such as nearby cars become well visible above clutter and the flying targets becomes easier to identify at far range (Fig. 10). Various kinds of planes, including large commercial aircrafts (Fig. 9, left) as well as smaller two-seat training aircraft and helicopters have been detected in this way. The measurement sequences are limited by the data bandwidth which requires storing data in RAM rather than on a physical storage: at 2 MS/s, 4 bytes/sample, two channels and I/Q coefficients, the datarate is 32 MB/s or 1.92 GB/minute. Due

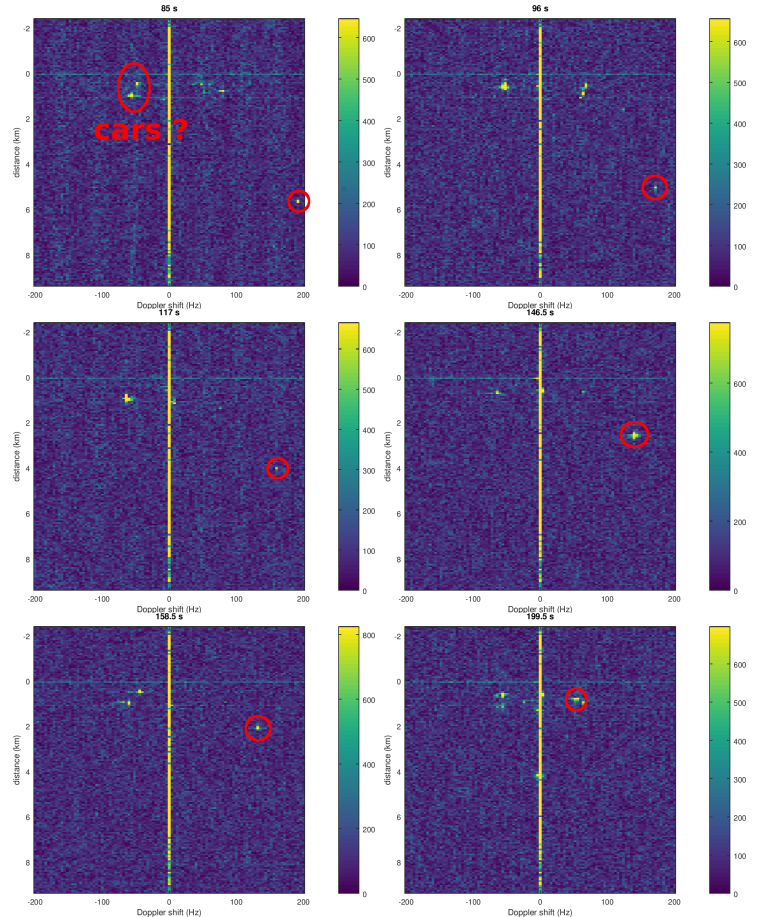


Fig. 10. Left: picture of a plane landing in front of the antenna collecting the measurements. Right: evolution of the range (Y-axis)-velocity (X-axis) map over time as the plane approaches and lands. The bright cross being the clutter sidelobes in the range and velocity directions. Time evolves from top-left (plane furthest from landing strip at the lower-right of the picture) to bottom-right (plane over the landing strip).

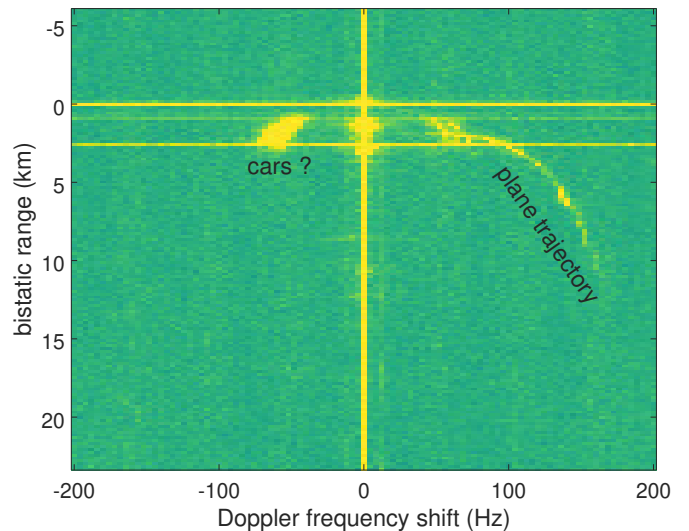


Fig. 11. Integrating over time the range-Doppler maps provides a full picture of the plane velocity and range during descent.

to storage limitations, all sequences were at most 4 minute long.

As an illustration of the identification of the range and velocity analysis during plane landing, the range-Doppler maps are stacked to give a complete picture (Fig. 11).

Clutter removal using a least-square method allows for identifying the remote target more clearly (Fig. 12), but most sig-

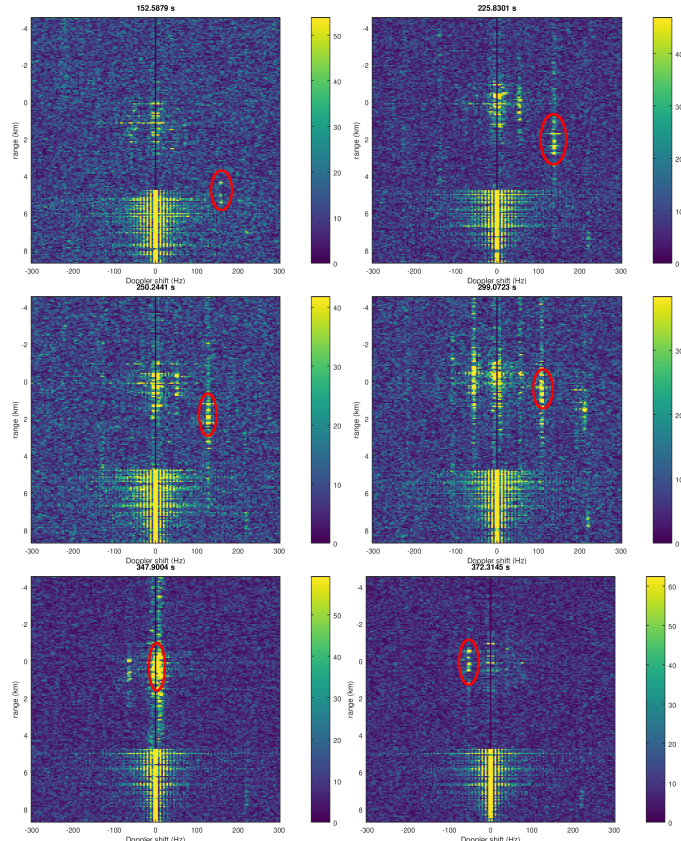


Fig. 12. Plane landing sequence, different from the one shown in Fig. 12, with clutter removal using a least-square method.

nificantly helps identify nearby targets at a range of about 1 km and exhibiting Doppler shifts in the ± 70 Hz range, consistent with cars driving on a bridge at speeds of about 70 km/h. In this application, the observation matrix A is assembled by time-delayed copies of the reference signal. Considering N samples of the reference and measurement signals are considered in the ambiguity function calculation, and P delays are considered for removal of clutter, then A is a $N \times P$ matrix. In our case, $N = 2.5 \cdot 10^5$ and $P = 128$. The measurement dataset $meas'$ used now in the ambiguity function calculation then becomes $meas' = meas - A \cdot pinv(A) \cdot meas$ with $pinv(A)$ the pseudo-inverse $(A^t \cdot A)^{-1} \cdot A^t$ where t indicates the transpose of the matrix. Since the identification of the time-delayed copies of the reference signal in the measurement signal is not perfect, some of the delayed reference signal subtracted from the measurement signal will spread in the range-direction the ambiguity function, as seen on Fig. 12.

B. Ship detection

Ships entering and leaving the port of Sendai have been observed using passive radar. While our initial aim was to focus on large RCS ships such as ferryboats and container ships, we observe multiple short range fast targets whose source has not been identified. Fig. 13 exhibits one measurement result, in which three ships are visible on the horizon. Two of the ships are moving in opposite directions with respect to the antennas, while the third one has been observed to be static during the whole measurement duration. Because ships move slower than planes, a strategy was devised to extend acquisition duration: despite GNURadio processing floating point numbers, the DVB-T receivers only sample 8-bit data. Hence, the complex values provided to GNURadio, ranging between -1 and +1, are scaled by 127 and stored as interleaved

8-bit integers, multiplying by 4 the acquisition duration which here lasts up to 12 minutes. The ship motion is clearly visible over such a long duration. Indeed, at a Doppler shift of about 12 Hz, the radial velocity is 3.6 m/s or 13 km/h and the motion over 12 minutes is 2.6 km along the radial direction.

The shorter range target, still resolved with the 75 m range resolution of the 2 MHz wide DVB-T receivers, are also visible on Fig. 13 at a range of about 1.8 km but with Doppler shifts up to 25 Hz, hinting at radial velocities up to 7.5 m/s or 27 km/h.

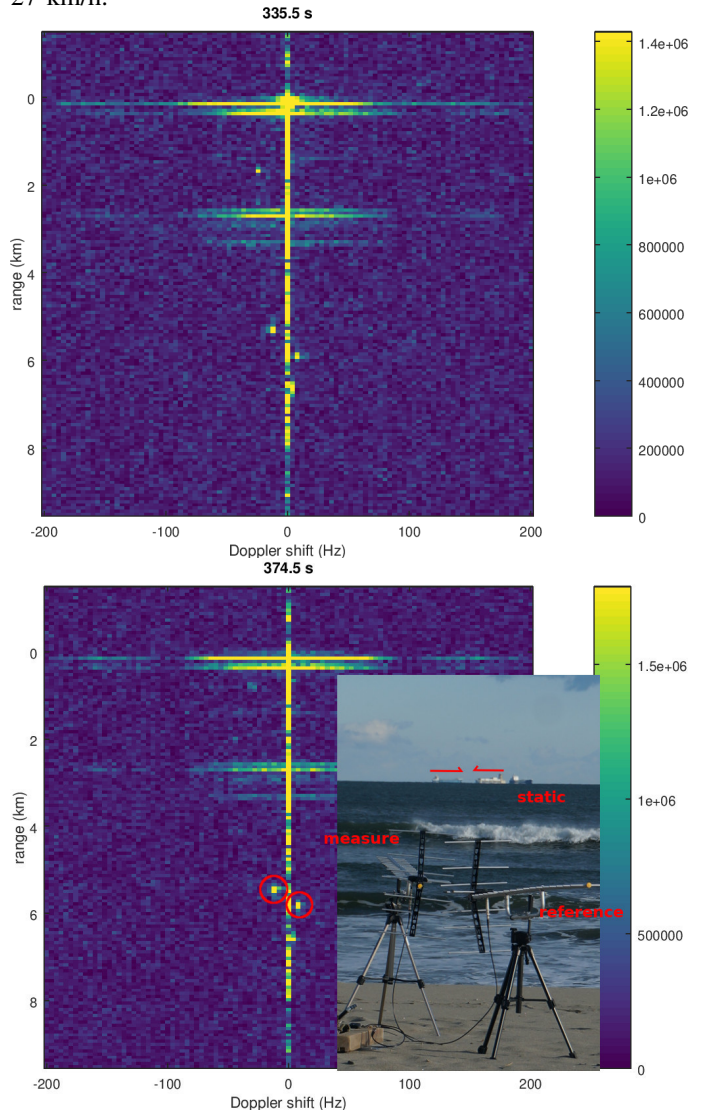


Fig. 13. Large ship detected from the beach next to the Sendai port. Three ships are seen from the beach: two moving in opposite directions, and one static (right inset). The two range-Doppler maps are separated by 40 s.

V. APPLICATION TO SHORT RANGE MOVING TARGET DETECTION

The final application considered for low-cost DVB-T receiver based passive radar measurements is near-range target detection. Since the 2 MHz-bandwidth receivers only allow for a range resolution of 75 m, observing low RCS such as cars or motorbikes does not allow for range measurement. Hence, setting the range to $\tau = 0$ in the ambiguity function Eq. 1 becomes $x(f_D) = \int_{-\infty}^{+\infty} ref(t) \cdot mes^*(t) \exp(j2\pi f_D t) dt$ which is the Fourier transform of the product of the reference signal and the complex conjugate of the measurement signal. Integrating long enough to achieve both improved signal to

noise ratio through increased pulse compression, and higher Doppler-frequency resolution, allows for using time-segments 0.5 s long. Fig. 14 exhibits one three-minute long dataset analysis, with various vehicles driving towards or away the measurement antenna inducing positive or negative Doppler shifts (Y-axis). While acquiring the data, a movie of the road was recorded, from which 1 frame per second was extracted. Manual deletion of the pictures without moving targeted yielded a selection of busses, cars and motorbikes which drove in front of the receiving antenna during the 3-minute long record. Each white line on the bottom of the chart of Figs. 14 and 15 is associated with one vehicle.

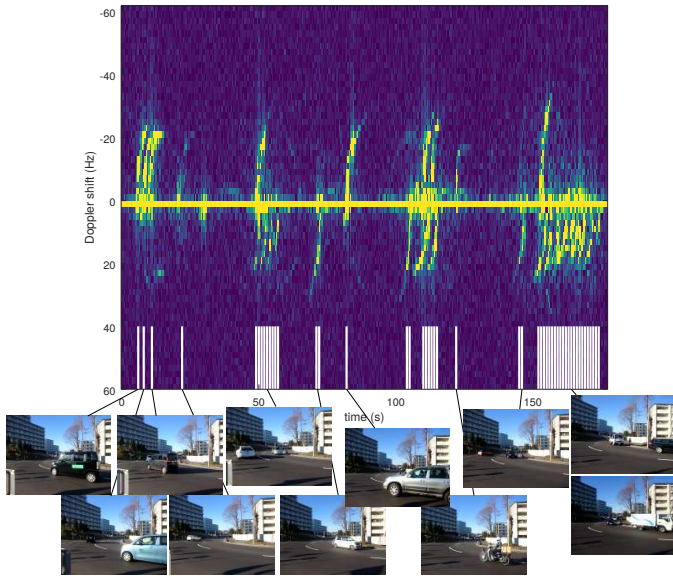


Fig. 14. Top: Doppler evolution (Y-axis) of targets driving in front of the receiving radar antenna as a function of time (X-axis). Bottom: selection of a few pictures from a movie recorded while acquiring radar data, illustrating some of the white lines on the bottom part of the top graph indicating each time a vehicle is visible in the movie.

Fig. 15 exhibits another resulting dataset, with the Doppler shift in the Y-axis and slow-time evolving in the X-axis.

The first vehicle in Fig. 15 is a motorbike: the MTI analysis is efficient enough to allow for detecting such a low RCS target. The fourth target from right is a car leaving a parking and driving away from the receiving antenna, indicating that the range of the measurement is extended enough that the target does not need to drive right in front of the receiving antenna.

Here again the observed Doppler shift is coherent with vehicles turning at a speed of 30 km/h, and Doppler shift sign varying whether the target drives towards or away from the receiving antenna. All non-zero Doppler traces are associated with a vehicle, and all vehicles in the movie are associated with a radar trace. Hence, the two measurement techniques appear complementary, with the radar measurement providing a quantitative measurement of the vehicle speed and the picture providing a qualitative information of target presence.

VI. CONCLUSION

Using consumer-grade DVB-T receivers as general purpose software defined radio receivers applied to passive radar detection has been demonstrated. We have exhibited the processing steps needed to develop the experimental setup, namely feeding both receivers with a common clock and tuning the

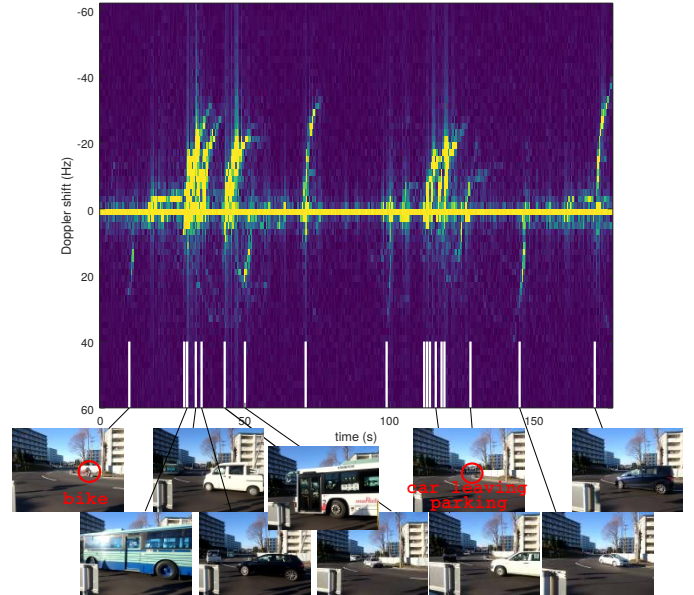


Fig. 15. Top: Doppler evolution (Y-axis) of targets driving in front of the receiving radar antenna as a function of time (X-axis). Bottom: selection of a few pictures from a movie recorded while acquiring radar data, illustrating some of the white lines on the bottom part of the top graph indicating each time a vehicle is visible in the movie.

phase locked loop to disable dithering. The time offset between the two datastreams remains constant and is calibrated since the delay introduced by the USB-bus is not deterministic and changes during each experiment. No sample loss was observed for sampling rates lower than 2.048 MS/s.

Despite the low range resolution of such a low bandwidth, various far-range and short range, static and moving targets, were detected. The Moving Target Indicator analysis allowed for detecting planes at a range of 4 km or cars at short, undetermined, range.

Extending the setup to include more receiving antennas and hence allow for azimuth detection, as proposed for example with the hardware setup available from <https://coherent-receiver.com/>, will provide an improved target identification with range, velocity and azimuth identification.

ACKNOWLEDGEMENT

J.-MF is grateful to the National University Corporation Tohoku University for granting an appointment as a 3-month visiting scientist to the Center for Northeast Asian Studies. The DVB-T passive radar investigation is partly supported by the French Centre National de la Recherche Scientifique (CNRS) PEPS grant.

REFERENCES

- [1] http://rtlsdr.org/#history_and_discovery_of_rtlsdr, accessed Dec. 2017.
- [2] H. A. Harms, L. M. Davis, and J. Palmer, "Understanding the signal structure in DVB-T signals for passive radar detection," in *IEEE Radar Conference*, 2010, pp. 532–537.
- [3] A. Evers and J. A. Jackson, "Cross-ambiguity characterization of communication waveform features for passive radar," *IEEE Transactions on Aerospace and Electronic Systems*, vol. 51, no. 4, pp. 3440–3455, 2015.
- [4] Z. Gao, R. Tao, Y. Ma, and T. Shao, "Dvb-t signal cross-ambiguity functions improvement for passive radar," in *Radar, 2006. CIE'06. International Conference on*. IEEE, 2006, pp. 1–4.
- [5] kaira.sgo.fi/2013/09/passive-radar-with-16-dual-coherent.html, accessed Dec. 2017.
- [6] www.rtl-sdr.com/building-a-passive-radar-system-with-an-rtl-sdr.
- [7] <https://www.youtube.com/watch?v=KRqtqCVRRO>.
- [8] <https://www.youtube.com/watch?v=I9V73d0nF4A>.
- [9] <http://superkuh.com/rtlsdr.html>, accessed Dec. 2017.